Erschienen in: Molecular Biology of the Cell ; 28 (2017), 12. - S. 1591-1600
https://dx.doi.org/10.1091/mbc.E16-10-0707

Twitchin kinase inhibits muscle activity

Yohei Matsunaga[a], Hyundoo Hwang[b,†], Barbara Franke[c], Rhys Williams[c], McKenna Penley[d], Hiroshi Qadota[a], Hong Yi[e], Levi T. Morran[d], Hang Lu[b], Olga Mayans[c], and Guy M. Benian[a,*]
[a]Department of Pathology, [d]Department of Biology, and [e]Apkarian Integrated Electron Microscopy Core, Emory University, Atlanta, GA 30322; [b]School of Chemical and Biomolecular Engineering, Georgia Institute of Technology, Atlanta, GA 30332; [c]Department of Biology, University of Konstanz, 78457 Konstanz, Germany

ABSTRACT **Muscle sarcomeres contain giant polypeptides composed of multiple immunoglobulin and fibronectin domains and one or two protein kinase domains. Although binding partners for a number of this family's kinase domains have been identified, the catalytic necessity of these kinase domains remains unknown. In addition, various members of this kinase family are suspected pseudokinases with no or little activity. Here we address catalytic necessity for the first time, using the prototypic invertebrate representative twitchin (UNC-22) from *Caenorhabditis elegans*. In in vitro experiments, change of a conserved lysine (K) that is involved in ATP coordination to alanine (A) resulted in elimination of kinase activity without affecting the overall structure of the kinase domain. The same mutation, *unc-22(sf21)*, was generated in the endogenous twitchin gene. The *unc-22(sf21)* worms have well-organized sarcomeres. However, *unc-22(sf21)* mutants move faster than wild-type worms and, by optogenetic experiments, contract more. Wild-type nematodes exhibited greater competitive fitness than *unc-22(sf21)* mutants. Thus the catalytic activity of twitchin kinase has a role in vivo, where it inhibits muscle activity and is likely maintained by selection.**

Monitoring Editor
Laurent Blanchoin
CEA Grenoble

Received: Oct 11, 2016
Revised: Apr 4, 2017
Accepted: Apr 11, 2017

INTRODUCTION

Sarcomeres, the fundamental units of muscle contraction, contain giant polypeptides (>700,000 Da) composed primarily of multiple copies of immunoglobulin (Ig) and fibronectin type 3 (Fn) domains, one or two protein kinase domains, and, in some proteins, highly elastic unique regions (Kontrogianni-Konstantopoulos *et al.*, 2009). Members of this family include titin and obscurin in mammals; twitchin, UNC-89, and TTN-1 in nematodes; twitchin in molluscs; and projectin, Unc-89, sallimus, and stretchin in insects. Despite the different sources of these proteins and differences in their overall lengths, nearly all have a conserved kinase region with the same arrangement of domains surrounding the protein kinase domain, namely, Fn-NL-kinase-CRD-Ig (NL and CRD denote N- and C-terminal regulatory kinase tail domains, respectively; Mayans *et al.*, 2013). The crystal structure of the largest segment containing a kinase domain from any of these giant polypeptides is from *Caenorhabditis elegans* twitchin kinase, namely, Fn-NL-kinase-CRD-Ig (von Castelmur *et al.*, 2012). In this, both NL and CRD segments pack against the kinase domain, inhibiting its catalysis (von Castelmur *et al.*, 2012). The 60-residue CRD tail is wedged between the two kinase subdomains, blocking sites for ATP binding, substrate recognition, and catalysis; the 45-residue NL forms a "crown" resting on the back of the hinge between the two kinase lobes.

Much is known about these proteins, especially for titin, with regard to their binding partners and roles in sarcomere assembly, muscle elasticity, and sensing and transduction of mechanical signals (Gieseler *et al.*, 2016; Krüger and Kötter, 2016; Krüger and Linke, 2011). However, the in vivo substrates and physiological functions of the kinase domains in these proteins are largely unknown. In vitro, *Aplysia* twitchin kinase can phosphorylate regulatory myosin light chains (Heierhorst *et al.*, 1996). In vitro, the C-terminal protein kinase of mouse obscurin can phosphorylate N-cadherin (Hu and Kontrogianni-Konstantopoulos, 2013). However, it is unclear whether these substrates are physiologically relevant. Moreover, it is even unknown whether some of these kinase domains might be catalytically active in vivo. In this respect, there is evidence that titin kinase (Bogomolovas *et al.*, 2014) and kinase PK1 from *Drosophila*

This article was published online ahead of print in MBoC in Press (http://www.molbiolcell.org/cgi/doi/10.1091/mbc.E16-10-0707) on April 20, 2017.

†Present address: School of Engineering and Sciences, Tecnologico de Monterrey, Monterrey, NL 64849, Mexico.

*Address correspondence to: Guy M. Benian (pathgb@emory.edu).

Abbreviations used: DSF, differential scanning fluorimetry; DTT, dithiothreitol; EIGC, Emory Integrated Genomics Core; EM, electron microscopy; Fn, fibronectin; GFP, green fluorescent protein; Ig, immunoglobulin; PDMS, polydimethylsiloxane; SAXS, small-angle x-ray scattering.

Supplemental Material can be found at:
http://www.molbiolcell.org/content/suppl/2017/04/17/mbc.E16-10-0707v1.DC1

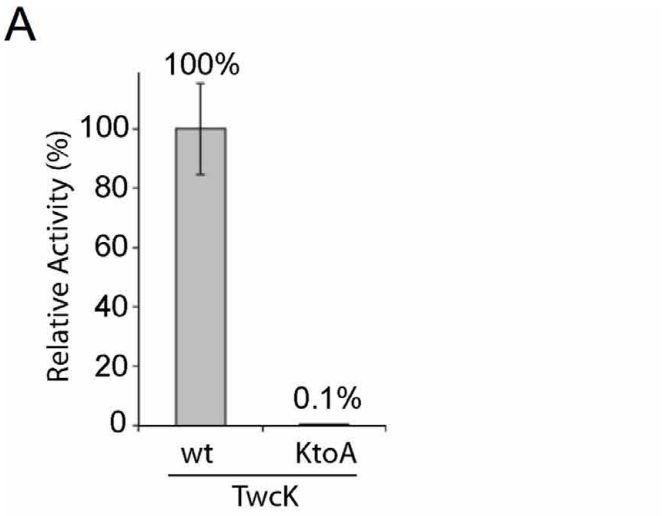

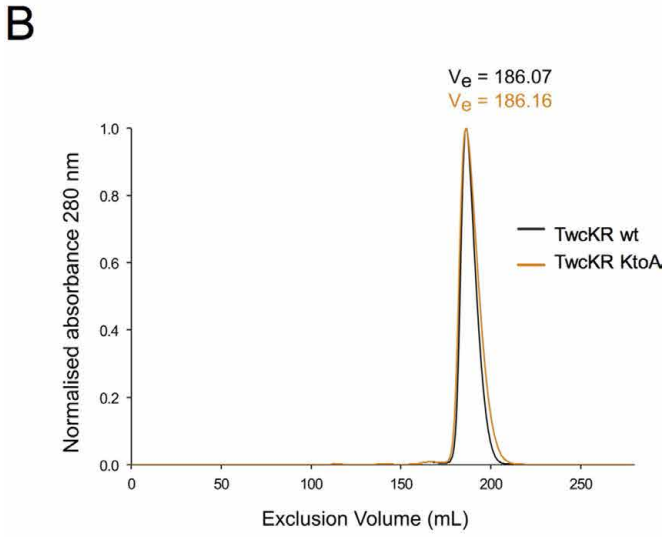

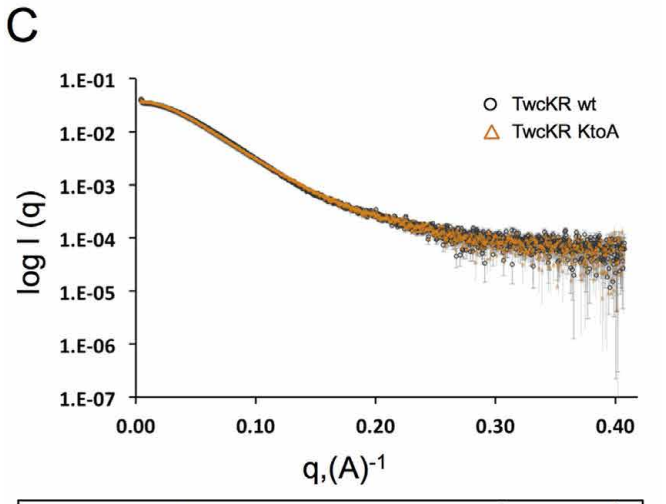

	MM^{calc} (kDa)	MM^{exp} (kDa)	Rg (Å)	D_{max} (Å)
TwcKR wt	66.1	55.0	31.79±2.47	120
TwcKR KtoA	66.1	57.0	33.12±1.28	122

FIGURE 1: Mutation of a lysine involved in ATP coordination/phosphotransfer to alanine (K6290A) eliminates catalytic activity but has no effect on the overall structure of twitchin kinase in vitro. (A) The wild-type (wt) and the K6290A mutant forms of the catalytic domain of twitchin kinase (TwcK) were each expressed and purified from *E. coli*. The ability to phosphorylate a model peptide was measured with [γ-^{32}P]ATP. As shown, the K6290A mutation almost entirely eliminates catalytic activity. (B) Size exclusion chromatograms of wt and mutant forms of a larger construct, TwcKR (Fn-NL-kin-CRD-Ig). TwcKR wt and TwcKR KtoA samples are coincident within experimental error, supporting the structural similarity of the samples. (C) SAXS analysis shows that the K6290A mutation does not affect the overall structure of the twitchin kinase region (TwcKR), so that the arrangement of assembled domains remains unaltered. Experimental scattering curves from TwcKR wt (black circle; capped error bars) and TwcKR K6290A (orange triangles; uncapped error bars) were scaled using DATADJUST (Petoukhov *et al.*, 2012). The table below the graph lists molecular parameters calculated from the scattering data. MM, R_g, and D_{max} denote molecular mass, radius of gyration, and maximal particle size, respectively. MM^{calc} is the theoretical MM of the constructs computed from primary sequence. R_g was calculated using AUTORG (Petoukhov *et al.*, 2007).

Unc-89 (Mayans *et al.*, 2013) may be inactive pseudokinases. In addition, a number of scaffolding interactions have been reported for this family of giant kinases, which leads to the question of whether it is scaffolding and not catalysis that is of functional relevance for these kinase domains. For example, in cultured cardiomyocytes, partially open forms of titin kinase differentially bind to several proteins (autophagosome receptors p62 and Nbr1 and the E3 ubiquitin ligase MuRF2), and this leads to activity-dependent translocation of serum response factor, resulting in increased sarcomeric gene expression (Lange *et al.*, 2005). Both protein kinase domains of nematode UNC-89 bind to SCPL-1, a CTD-type phosphatase (Qadota *et al.*, 2008). Nematode twitchin kinase binds to and is phosphorylated by MAPKAP kinase 2 in vitro (Matsunaga *et al.*, 2015). In *Drosophila* Unc-89, kinase domain 1 interacts with Ballchen (a protein kinase), and both kinase domains 1 and 2 interact with MASK (an ankyrin repeat protein; Katzemich *et al.*, 2015).

To bring light to this debate, we explore for the first time the catalytic significance of a muscle giant kinase, twitchin kinase, in vivo. Using clustered regularly interspaced short palindromic repeats (CRISPR)/Cas9 gene-editing technology, we created a *C. elegans* strain that expresses, as its sole source of twitchin, one that contains an intact but catalytically inactive protein kinase. Although nematodes expressing twitchin with a catalytically inactive kinase domain have normal sarcomere organization, remarkably, they move faster than wild-type nematodes. Our results demonstrate for the first time that twitchin kinase activity is required for normal muscle function and is involved in a pathway regulating muscle contraction.

RESULTS AND DISCUSSION

Conversion of catalytic lysine to alanine abolishes protein kinase activity and does not affect the structure of the protein kinase domain in vitro

The catalytic protein kinase domain of twitchin (TwcK) is active in in vitro phosphortransfer assays against a model peptide substrate (Lei *et al.*, 1994; von Castelmur *et al.*, 2012). A highly conserved lysine in the small lobe of protein kinases coordinates ATP and helps transfer the γ-phosphate. Mutation of this lysine into alanine or several other amino acids inactivates many known kinases (e.g., Iyer *et al.*, 2005b). We purified bacterially expressed recombinant twitchin TwcK in wild-type form and as a mutant in which this lysine (residue 6290 in full-length twitchin, UNC-22B) was converted to an alanine (K6290A). As shown in Figure 1A, in an in vitro kinase assay, TwcK K6290A shows barely detectable phosphotransferase activity; it displays ~0.1% of wild-type activity.

Conversion of the catalytic lysine to alanine is not known to influence the overall fold of a kinase domain. Nevertheless, we investigated whether the K6290A mutation in the twitchin kinase domain would have an effect on its structure as well as on the overall assembled conformation of the kinase region, thereby validating that the NL and CRD tails remained bound to the kinase and that long-range alterations of the area had not taken place. For this purpose, we studied a larger segment of twitchin that included flanking domains, Fn-NL-kin-CRD-Ig (TwcKR). The expression, yield, and solubility of recombinant TwcKR K6290A were nearly identical to those of TwcKR wild type. In addition, the wild-type and K6290A mutant forms of recombinant TwcKR behaved indistinguishably on size exclusion chromatography, suggesting that the samples share an overall shape and surface chemistry (Figure 1B). The overall molecular features of twitchin kinase in its wild-type and KtoA mutant forms were further studied using small-angle x-ray scattering (SAXS). The experimental scattering curves from these samples (Figure 1C), as well as their corresponding radius of gyration (R_g) and maximum dimension (D_{max}) values (Figure 1C), are in agreement within the error of this technique. This suggests that both TwcKR forms share a similar global conformation and that the introduction of the K6290A mutation does not detectably affect the conformation of twitchin.

Differential scanning fluorimetry (DSF) was used to assess the effect of the K6290A substitution on TwcKR thermal stability. Results revealed T_m values of 44 and 41°C for TwcKR wild-type and TwcKR K6290A, respectively (Supplemental Figure S1). The decrease in thermal stability (ΔT_m) of −3°C observed for TwcKR K6290A is comparable to that recorded for the exchange KtoL in titin kinase (ΔT_m = −2.2°C; Bogomolovas *et al.*, 2014) and noticeably smaller than that of an equivalent KtoA mutation in titin kinase (ΔT_m = –6.6°C; Bogomolovas *et al.*, 2014) or a KtoH mutation in cAMP-dependent protein kinase (PKA; ΔT_m = −10.7°C; Iyer *et al.*, 2005a). None of these other exchanges was known to have functional consequences—even the most destabilizing KtoH substitution in PKA, although it abolished the catalytic activity of PKA, did not affect substrate or regulatory subunit binding (Iyer *et al.*, 2005b). Furthermore, structural studies on mutated protein variants showing decreased thermal stabilities of up to ~10°C found that fold alterations are rarely detectable in such cases. As an example, a nuclear magnetic resonance study of a variant of domain I10 from titin carrying the exchange T2850I ($\Delta T_m \approx -11$°C) did not reveal any significant structural alteration—globally or locally (Bogomolovas *et al.*, 2016). In the crystal structure of TwcKR (von Castelmur *et al.*, 2012), the ε-amino group of the substituted K side chain interacts with the main-chain carboxyl group of residue Y6560 in the CRD. This interaction is abolished in TwcKR K6290A, possibly accounting for the slight decrease in thermal stability. However, SAXS experiments demonstrate that the K6290A substitution causes no detectable change to the conformation of TwcKR. In addition, the TwcKR K6290A T_m of 41°C remains significantly above the environmental temperature of *C. elegans* (15–25°C). Taken together, these data indicate that the K6290A substitution is unlikely to lead to artifactual structural effects in this in vivo study and that observations can be attributed to the lack of catalysis in this mutant.

Nematodes expressing twitchin with a catalytically inactive kinase domain (*unc-22(sf21)*) have normal sarcomere structure and normal response to nicotine and do not twitch

We next used CRISPR/Cas9 gene editing to create the same K6290A kinase domain mutation in the endogenous *unc-22* (twitchin) gene (Supplemental Figure S2). We outcrossed this mutant, designated *unc-22(sf21),* three times to wild type to remove most of the possible off-target mutations generated by CRISPR. We also sequenced the *unc-22* gene from this *unc-22(sf21)* strain and verified that no other mutations were present in the *unc-22* gene. We characterized the *unc-22(sf21)* phenotype as follows. In contrast to all previously characterized *unc-22* mutants (Moerman and Baillie, 1979; Moerman *et al.*, 1988; Matsunaga *et al.,* 2015), *unc-22(sf21)* animals do not twitch and show a wild-type response to nicotine (Supplemental Figure S3). Moreover, by Western blot, the *unc-22(sf21)* mutant expresses normal levels of various twitchin isoforms of the appropriate size (Supplemental Figure S4). The locomotion of nematodes arises from the alternating contraction and relaxation of body-wall striated muscles on its dorsal and ventral sides. By immunostaining with several antibodies to known sarcomeric proteins and visualization of thin filaments by phalloidin, we saw that the *unc-22(sf21)* mutant displays normal sarcomere structure in its body-wall muscle cells (Figure 2). This assessment includes the localization of twitchin, thick filament myosins (MYO-3, UNC-54), M-lines and dense bodies (UNC-95), and F-actin. This is in contrast to the loss of function *unc-22(e66)* and null *unc-22(ct37)* animals, which show disorganized sarcomeres (Supplemental Figure S5; *unc-22(e66)* is a 2–base pair deletion of coding sequence for Ig1, resulting in a frame shift and premature stop codon [unpublished data]; *unc-22(ct37)* is an intragenic deletion; and *unc-22(ct37)* animals show no detectable twitchin by Western blot [Moerman *et al.,* 1988]). The normal sarcomeric organization of the *unc-22(sf21)* mutant is a feature shared in common with the unusual allele *unc-22(e105)* (Matsunaga *et al.,* 2015; Supplemental Figure S5), which has a missense mutation in Ig7, changing a highly conserved glycine to an arginine (Matsunaga *et al.,* 2015). Nevertheless, *unc-22(e105)* is different from *unc-22(sf21)* in that, like all other known *unc-22* mutants, *unc-22(e105)* twitches and is resistant to nicotine (Supplemental Figure S3). The sarcomeric organization of *unc-22(sf21)* nematodes was examined at higher resolution by transmission electron microscopy (EM). As shown in Figure 3, the myofilament lattice of *unc-22(sf21)* appears indistinguishable from wild type; there are regularly organized A- and I-bands, normal-appearing dense bodies and M-lines, and normal-appearing thick and thin filaments.

To summarize, the *unc-22(sf21)* mutant expresses full-length twitchin isoforms that are stable and normally incorporated into sarcomeres, displays normal organization of sarcomeres, and neither twitches nor is resistant to nicotine.

unc-22(sf21) worms move faster than wild type and display abnormal muscle kinetics

Despite having no effect on muscle structure, the *unc-22(sf21*) mutation results in a remarkable effect on muscle function. Nematodes have different locomotion patterns, depending on the medium: in liquid, they thrash back and forth in a C-shaped pattern; on a semi-solid surface like agar, they crawl in a sinusoidal pattern. We measured the ability of adult nematodes to move back and forth in a droplet of aqueous buffer M9 (Epstein and Thomson, 1974). As shown in Figure 4A, when normalized to wild-type movement, worms with loss-of-function allele *unc-22(e66)* swam less well than wild type, and this is typical of nearly all *unc-22* alleles. However, *unc-22(sf21)* mutant worms, unexpectedly, moved ~30% faster than wild type; a similar increase in motility (up to 50% increase) was observed for *unc-22(e105)*. We also measured the ability of adult worms to crawl on an agar surface. As indicated in Figure 4B, these results are similar to those obtained with the swimming assay, in that *unc-22(e66)* nematodes crawl more slowly than wild type, but *unc-22(e105)* and especially *unc-22(sf21)* animals crawl faster than wild type.

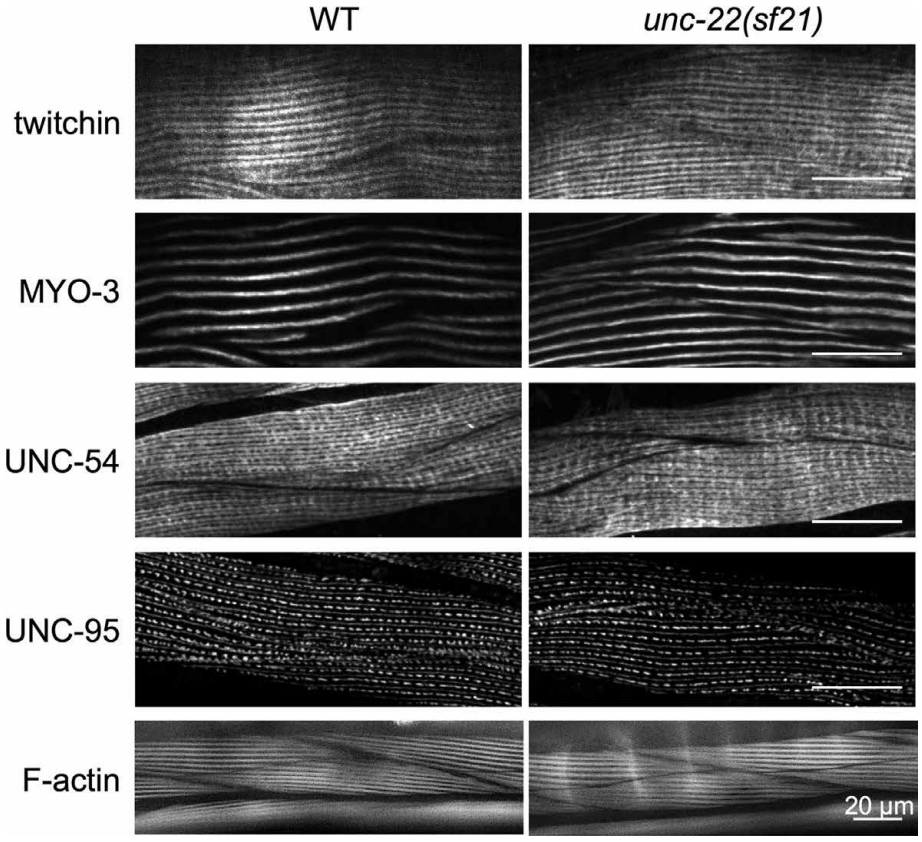

FIGURE 2: Nematodes expressing twitchin with the K6290A mutation in its kinase domain show normal muscle sarcomere structure, including normal localization of twitchin, by immunofluorescence microscopy. Wild-type (WT) and *unc-22(sf21)* mutant nematodes were fixed and immunostained with antibodies to the indicated sarcomeric proteins: twitchin, myosin heavy chain A (MYO-3), and myosin heavy chain B (UNC-54) of the A-bands and UNC-95 of M-lines and dense bodies. Phalloidin staining of F-actin of I-bands is also shown. As indicated, *unc-22(sf21)* shows normal localization of each sarcomeric protein tested, including twitchin. Scale bars, 20 µm.

Recently we adapted the use of optogenetics to obtain certain measures of contraction/relaxation kinetics of body-wall muscle in *C. elegans* (Hwang *et al.,* 2016). Channelrhodopsin-2 (ChR2) is expressed in motor neurons, and on exposure to blue light, contraction of all the body-wall muscles is induced at the same time. As a proxy of this contraction, we measure the relative body area of the worm, as shown in Figure 4C; by fitting curves, rate constants for contraction and relaxation can be derived. Figure 4D shows results of this assay on wild-type and three *unc-22* mutant alleles. As reported previously (Hwang *et al.,* 2016), *unc-22(e66)* nematodes (red line in Figure 4D) contract less well and cannot maintain a maximally contracted state. In contrast, both *unc-22(e105)* and especially *unc-22(sf21)* animals contract more deeply than wild type. Another measure from the optogenetic experiment in Figure 4D is the relative body area when muscles are maximally contracted (Figure 4G). In this measure, both *unc-22(e105)* and *unc-22(sf21)* nematodes contract more than wild type, whereas *unc-22(e66)* contracts less than wild type. Although the reduced contractility of *unc-22(e66)* nematodes may be explained by the disorganization of its myofilament lattice (Supplemental Figure S5), results for *unc-22(e105)* and *unc-22(sf21)* animals are puzzling. Either *unc-22(e105)* or *unc-22(sf21)* animals contract absolutely more, or they appear to contract more because they begin at a more relaxed state. Additional experiments will be required to distinguish these possibilities. In addition, all of the *unc-22* mutant strains show faster rates of contraction and relaxation (Figure 4, E and F). Given that the *unc-22(e66)* strain has the fastest rates for contraction and relaxation, we might expect that it would also swim and crawl at the highest velocity. However, this is not the case: *unc-22(e66)* animals swim and crawl at decreased velocities compared with wild type. Most likely, the slower movement of the *unc-22(e66)* nematodes is explained by the fact that they have disorganized sarcomeres so that the output is less efficient or the coordination of the muscle cells is impaired.

There is selective pressure to maintain kinase activity of twitchin

The fact that loss of twitchin kinase activity results in increased velocity of swimming and crawling, more muscle contraction, and faster rates of contraction and relaxation suggests that the normal function of twitchin kinase activity is to inhibit the contraction/relaxation cycle. Among invertebrates (*C. elegans*, *Drosophila*, *Aplysia*), twitchin and the similar protein projectin have active protein kinase domains, as determined by in vitro kinase assays (Lei *et al.*, 1994; Ayme-Southgate *et al.*, 1995; Heierhorst *et al.*, 1995, 1996; von Castelmur *et al.*, 2012). Therefore it seems that among invertebrates, there has been selection to maintain twitchin kinase activity. To test this hypothesis, we set up a "competitive fitness assay." We cultured 100 green fluorescent protein (GFP)–tagged test strain (JK2735) animals with 100 experimental animals (either *unc-22(sf21) 3X oc* or the N2 wild-type strain) and measured the frequency of the experimental strain after four generations of growth and reproduction in competition. If the strains exhibited equal levels of fitness, we would expect the 50% frequency to be maintained. Both the wild-type strain and *unc-22(sf21)* outcompeted the GFP-tagged tester strain (Figure 5A). However, the competitive fitness of *unc-22(sf21)* was significantly reduced relative to the wild-type strain (Figure 5A; $\chi^2_1 = 9.14$, $p = 0.0025$). Thus, at least in a laboratory setting, there is selective pressure to maintain the kinase activity of twitchin, despite its effect of reducing the overall locomotion of the animals. In support of our competition assay results, analysis of the sequences of twitchin orthologues from 47 nematode species, including *C. elegans*, showed that the six residues or segments crucial for catalysis, including the catalytic lysine (Endicott *et al.*, 2012; Mayans *et al.*, 2013), are conserved (Supplemental Figure S6).

We speculated that the poorer performance of *unc-22(sf21)* relative to wild-type N2 might be attributable to a reduction in brood size. As shown in Figure 5B, measurement of brood sizes indicate that, indeed, *unc-22(sf21)* has a smaller brood size than wild-type strain N2. One possibility for this reduced brood size is that twitchin is normally expressed in pharyngeal muscles (required for feeding and nutrition) and/or vulval or uterine muscles required for egg laying. Indeed, our promoter analysis (Supplemental Figure S7) indicates that several of the nine predicted twitchin mRNAs are expressed in pharyngeal and/or vulval muscles in addition to being expressed in body wall muscle. In addition, all of the isoforms are

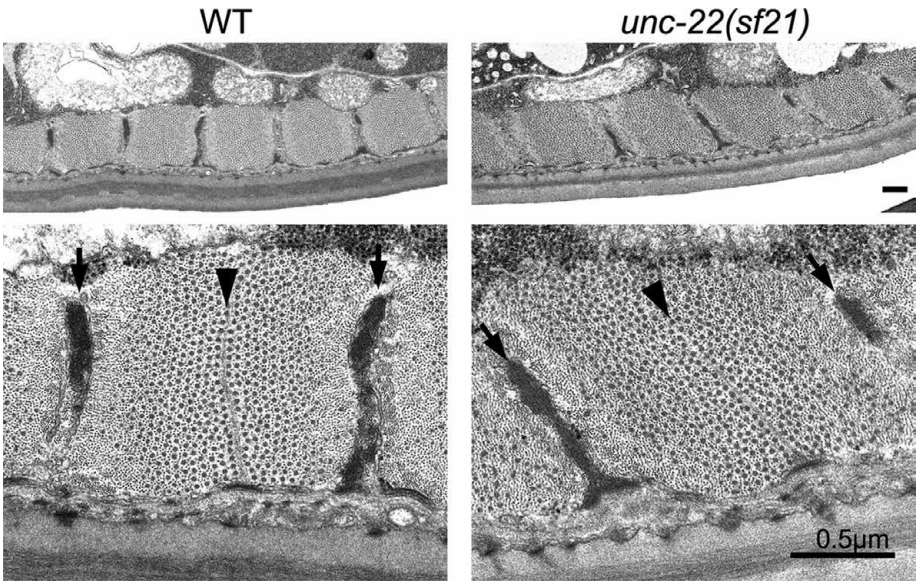

FIGURE 3: The *unc-22(sf21)* mutant shows normal sarcomere structure by EM. Transmission EM of a cross-section of a body-wall muscle cell from a wild-type (WT) animal and from an *unc-22(sf21)* mutant animal. Top, across most of the width of a single cell near the vulva, there is uniform depth of the contractile apparatus along the body wall and regular spacing of the filament attachment structures, and the thick and thin filaments are all cut in cross-section, demonstrating correct orientation of the filaments parallel to the body axis. Bottom, higher-magnification views show proper morphology and organization of attachment structures and interdigitating thick and thin filaments. Arrows point to dense bodies, and arrowheads point to M-lines. The largest black dots are cross-sections of thick filaments in the A-bands; the smallest dots are cross-sections of thin filaments. Scale bars, 0.5 µm.

predicted and/or verified to include the kinase domain. It also must be noted that the GFP-tagged strain (JK2735) has a smaller brood size than either N2 or *unc-22(sf21)*. The reduced brood size of the GFP strain explains why in the competition experiment, both N2 and *unc-22(sf21)* outcompeted the GFP strain. (The reduced brood size of JK2735 might be due to having GFP expressed in the pharynx, gut, and early embryo, thus interfering with feeding, nutrition, and/or development of this strain.)

Molecular dissection of twitchin functions

Until recently, all the *unc-22* mutants were reported to display several phenotypic characteristics, which vary in severity with mutant allele: 1) "twitching," which is abnormal constitutive fine movement along several portions of the body surface occurring approximately one to two times per second and originating from the underlying body-wall muscle; 2) resistance to the paralyzing effects of nicotine; 3) reduced locomotion; and 4) disorganization of sarcomeres (Moerman and Baillie, 1979; Moerman *et al*., 1988). Based on these phenotypes, twitchin is likely to have two functions: one in the assembly or maintenance of sarcomeres and the other in regulating muscle contraction. Whether these two functions are separate or related could not be discerned until now: all of the previously isolated alleles had some degree of each of the four phenotypes. Although the null allele, *ct37*, is an intragenic deletion (Moerman *et al.*, 1988), our sequence analysis of 10 additional *unc-22* mutants revealed that they all result in stop codons, either because they are simple nonsense mutations or because they are insertions/deletions that result in frameshifts and eventual stop codons (unpublished data). Until the study presented here, the one exception was *unc-22(e105)*, which twitches mildly and is resistant to nicotine but has normal sarcomere structure and moves faster than wild type (Matsunaga *et al.*, 2015). *e105* is a missense mutation in a highly conserved glycine (to arginine) in Ig7 and results in normal expression and localization of twitchin. Thus, because we can assume that all the Ig and Fn domains are present in *e105* mutant twitchin, we can conclude that the organization of sarcomeres and ability to locomote at normal (or better) velocity depends on the presence of these Ig and Fn domains. In the present study, we show that *unc-22(sf21)* animals, unlike *e105*, fail to twitch and have normal sensitivity to nicotine; however, like the *e105* worm, *unc-22(sf21)* has normal muscle structure and moves faster than normal. Thus we can conclude that one normal function of twitchin is to inhibit the muscle contraction/relaxation cycle, and this depends on the catalytic activity of the kinase domain. We do not know how to account for the phenotype of *e105*; we can speculate that perhaps twitchin's Ig7 inhibits the kinase domain in a twitchin dimer.

At this time, the mechanism by which twitchin kinase activity inhibits the contraction/relaxation cycle is unknown. A clue to this mechanism should arise from determining the substrate(s) for twitchin kinase, which we can now approach by using *unc-22(sf21)* mutant animals.

MATERIALS AND METHODS

Plasmids for expression of wild-type and K6290A mutant twitchin kinase

The plasmid for expression of histidine (His)-tagged wild-type twitchin kinase catalytic domain (TwcK) was described previously (von Castelmur *et al.*, 2012). The same catalytic domain (TwcK) with the K6290A mutation was amplified by PCR using primers TwiK-3 and TwiK-4 from an Fn-Kin-Ig K6290A template described in Matsunaga *et al.* (2015); the DNA sequence of this fragment was confirmed and then cloned into the pETM11 vector for expression as a His-tagged protein. The wild-type cDNA encoding Fn-NL-kin-CRD-Ig (TwcKR) was cloned into pET28 as described previously (Greene *et al.*, 2008) for expression as a His-tagged protein. The K6290A version of Fn-NL-kin-CRD-Ig (TwcKR K6290A) was created as described (Matsunaga *et al.*, 2015) and cloned into pET28.

Recombinant protein production

All twitchin kinase constructs (TwcK, TwcKR, wild type, and mutant at 6290) were expressed in *Escherichia coli* Rosetta 2 (DE3) (Merck Millipore) and grown in Luria–Bertani medium containing 25 µg/ml kanamycin and 34 µg/ml chloramphenicol. Growth was at 37°C to OD_{600} = 0.6–0.8, followed by induction of protein expression with 0.5 mM isopropyl β-D-1-thiogalactopyranoside and further growth at 18°C for ~18 h. Cell pellets were harvested by centrifugation and resuspended in 50 mM Tris-HCl, 500 mM NaCl, 1 mM dithiothreitol (DTT), pH 7.9 (lysis buffer), supplemented with 20 µg/ml DNase I (Sigma-Aldrich) and a complete EDTA-free protease inhibitor (Roche). Cell lysis was by sonication on ice, followed by clarification of the lysate by centrifugation.

In preparation for phosphotransfer assays, cell lysates were applied to Ni^{2+}-nitriloacetic acid (NTA) resin (Qiagen) equilibrated in

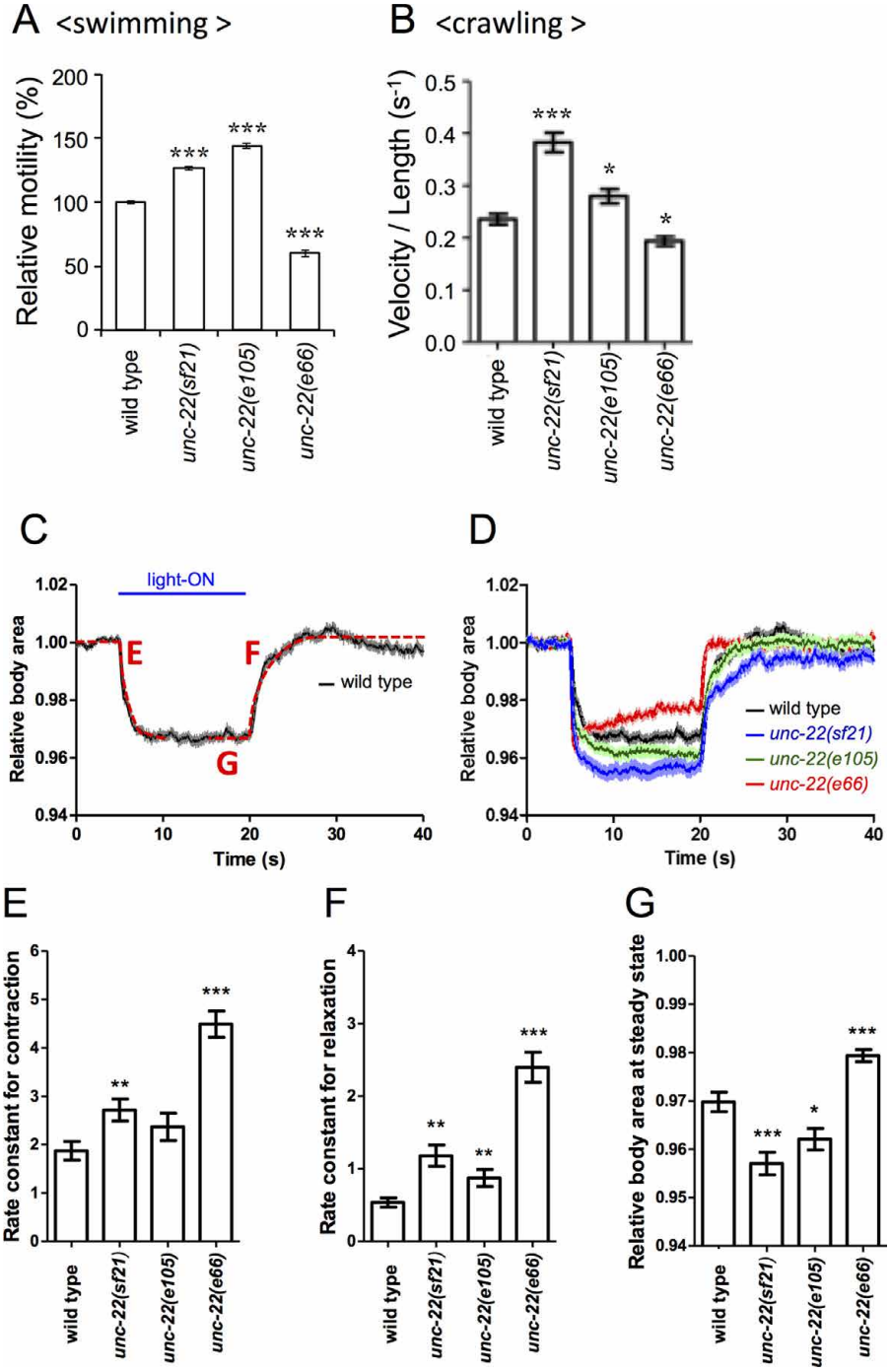

FIGURE 4: Nematodes lacking twitchin kinase activity move faster and show a greater degree of muscle contraction. (A) Results of a swimming assay in which the number of times an animal moves back and forth in liquid are counted. The slower motility of animals with the loss-of-function allele *unc-22(e66)* is typical of *unc-22* mutants. Both *unc-22(sf21)* and *unc-22(e105)* animals display, unexpectedly, faster motility. (B) Measurement of crawling velocity of nematodes on the surface of agar; results are normalized to the length of the animal. Results are similar to those obtained for swimming. (C) Typical results of an optogenetic experiment to measure contraction and relaxation of wild-type nematodes. Relative body area is a measure of the contraction state of body-wall muscle. (D) Optogenetic experiments on wild type and three *unc-22* mutants. Compared with wild-type animals, *unc-22(sf21)* and *unc-22(e105)* worms display a greater degree of muscle contraction, whereas *unc-22(e66)* worms show less muscle contraction and an inability to maintain the contracted state. (E, F) Rate constants for contraction ("E" in C) and for relaxation ("F" in C) derived from fitting curves to data shown in D. (G) Relative body area at steady state, which is the average relative body area during 5 s before the relaxation ("G" in C). These numbers emphasize that *unc-22(sf21)* and *unc-22(e105)* nematodes contract more than wild type. For A, B, and E–G, $n > 40$; *$p < 0.01$, **$p < 0.001$, and ***$p < 0.0001$.

lysis buffer containing 20 mM imidazole. Elution was with 200 mM imidazole, and samples were buffer exchanged into lysis buffer using PD-10 desalting columns (GE Healthcare). The His_6-tag removal was by TEV protease cleavage overnight at 4°C, followed by subtractive Ni^{2+}-NTA purification. Size exclusion chromatography was carried out using a Superdex 200 16/60 column (GE Healthcare) in 50 mM Tris-HCl, 50 mM NaCl, and 1 mM DTT, pH 7.9.

In preparation for SAXS and DSF, cell lysates were applied to a 5-ml HisTrap HP column (GE Healthcare) equilibrated in lysis buffer containing 20 mM imidazole. Elution of His_6-tagged protein was by continuous imidazole gradient, followed by buffer exchange into 50 mM Tris-HCl, 50 mM NaCl, and 1 mM DTT, pH 7.9 (anion exchange buffer), His_6-tag cleavage by TEV protease, and subtractive Ni^{2+} purification. Anion exchange was performed using a 5-ml QFF column equilibrated in anion exchange buffer (GE Healthcare) with elution by continuous NaCl gradient. Size exclusion chromatography was carried out using a Superdex 200 26/60 column (GE Healthcare) in 50 mM Tris-HCl, 50 mM NaCl, and 0.5 mM tris (2-carboxyethyl)phosphine (TCEP), pH 7.9.

In vitro phosphotransfer assay

In vitro phosphotransfer assays were set up in 40-µl reactions containing 30 ng of TwcK and 20 mM Tris-HCl, pH 7.4, 10 mM $MgCl_2$, 0.2 mg/ml bovine serum albumin, and 0.2 mg/ml peptide substrate. Reactions were initiated by addition of 200 µM [γ^{32}P] ATP (2 µCi per reaction). The peptide substrate has the sequence KKRARAATSNVFS and is a model peptide substrate derived from chicken myosin light chain (kMLC11-23) as described (Heierhorst *et al.*, 1996; von Castelmur *et al.*, 2012). Control reactions were included in all assays containing peptide substrate in the absence of TwcK and with TwcK in the absence of peptide substrate. Incubation of samples was at 25°C for 20 min before blotting on P81 phosphocellulose paper and submergence in 100 mM phosphoric acid to terminate reactions. Blotted samples were washed four times in 100 mM phosphoric acid for 5 min/wash before being transferred to acetone and air dried. Quantification was by Cherenkov counting using a Beckman Coulter scintillation counter.

Small-angle x-ray scattering

SAXS data were collected at the B21 beamline of the Diamond Light Source synchrotron (Didcot, United Kingdom) using the integrated SEC-SAXS setup, including the

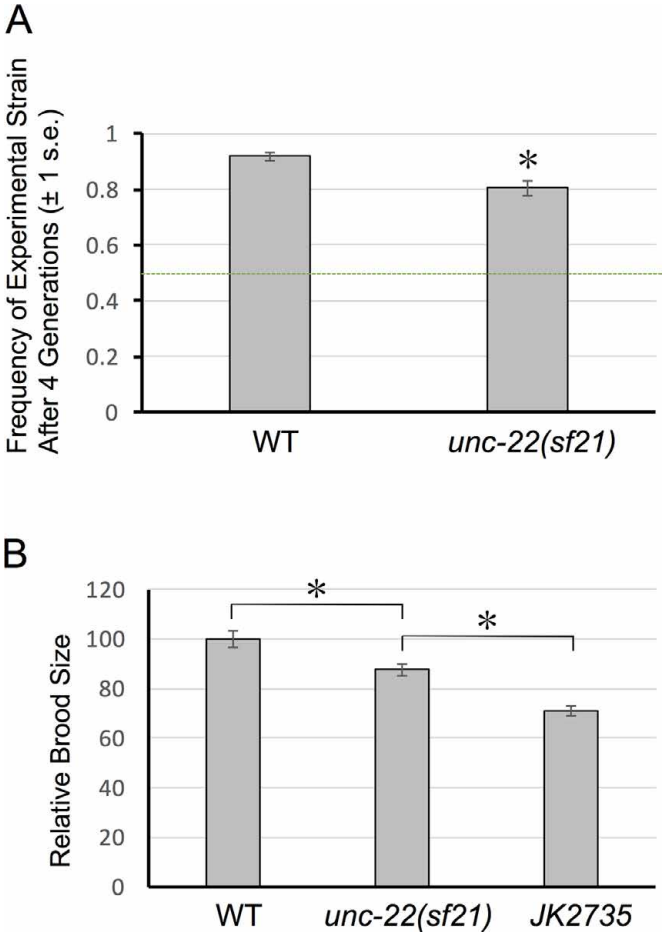

FIGURE 5: A competition assay demonstrates that the *unc-22(sf21)* mutant has a selective disadvantage relative to wild type. (A) Competition assay results. Equal numbers of GFP-tagged wild-type ("tester" strain, JK2735) and the indicated strains were cultured on plates with *E. coli* food, and after four generations, the frequency of each strain was determined. (B) Relative brood sizes of wild-type strain N2, *unc-22(sf21)*, and GFP-tagged strain (JK2735). *Significance with $p < 0.05$.

HPLC device Agilent 1260C. Approximately 1–1.2 mg of sample (TwcKR wild type, TwcKR KtoA) was loaded in 45 µl of buffer (50 mM Tris, pH 7.9, 50 mM NaCl, 0.5 mM TCEP) onto a preequilibrated Shodex KW403 column at a flow rate of 0.16 ml/min. Frames were collected for the entire eluate using a exposure time of 3 s/frame and a sample cell thermostated to 20°C. The x-ray scattering was recorded on a Pilatus 2 M detector (Dectris) at a sample-to-detector distance of 3.9 m and a wavelength of 1 Å. Data processing used ScÅtter (www.bioisis.net/tutorial/9; Diamond, unpublished). Scattering curves were analyzed with PRIMUS (Konarev *et al.*, 2003) and the ATSAS software suite (Petoukhov *et al.*, 2012) to determine R_g, D_{max}, and the pair distribution function, $P(r)$. The experimental molecular mass was calculated using ScÅtter (Rambo and Tainer, 2013).

Differential scanning fluorimetry

DSF assays were performed using a CFX connect Real-Time PCR machine (Bio-Rad) with a thermal ramping of 1°C/min in the temperature range 25–95°C. Proteins were tested at a concentration of 7.5 µM in 50 mM Tris-HCl, pH 7.9, 50 mM NaCl, and 0.5 mM TCEP. SYPRO-orange dye (Invitrogen) was diluted to a concentration of 1:1000 in the same buffer. Assays were carried out in a volume of 25 µl and in triplicate. Data were processed using CFX Manager software (Bio-Rad), and T_m values were calculated from the first derivative of the melting curves.

Nematode strains

N2 (Bristol) is the primary wild-type strain, and standard growth conditions were used (Brenner, 1974). The following alleles were used in this study: *unc-22*(*e66*)IV, *unc-22*(*e105*)IV, *unc-22*(*ct37*)IV, and *zxIs6[unc-17p::ChR2(H134R)::YFP; lin15⁺]V* (Liewald *et al.*, 2008). *unc-22(sf21); zxIs6* was generated by crossing. To check for mutations of mutant animals, we carried out single-worm PCR. After purification of PCR products, we examined a restriction enzyme digestion (*Pst*I) and DNA sequence analysis to verify the mutation.

Creation of *unc-22(sf21)* animals

The K6290A mutation in the coding sequence of the endogenous *unc-22* gene was generated using a CRISPR technique as described (Paix *et al.*, 2015). For targeting to *unc-22*, a sequence, 5′-actccacatgaatctgaca-3′ was cloned into pDD162 (Addgene plasmid 47549) using a Q5 site-directed mutagenesis kit (New England BioLabs). To modify the genome using Cas9 triggered homologous recombination, the following DNA mixtures were injected: 50 ng/µl pDD162 with targeting sequences, 30 ng/µl single-strand oligo 5′-aactggaaacaactttgctgcagcattcgtaatgactccacatgaatccgacaaagaaactgtcagaaaagagattcaaaccatgtcagttttgagacac-3′ as repair template, and 30 ng/µl pTG96 (Yochem *et al.*, 1998) as coinjection marker. For screening of the mutants, we picked single F1 animals to PCR tubes and performed single-worm PCR using the primers 5′-tgaaccaccaagattcccgattatc-3′ and 5′-ccaacgctccacatatcggtg-3′. After purification of PCR products, we examined a restriction enzyme digestion (*Pst*I) and performed DNA sequence analysis to verify the mutation. The homozygous mutant was outcrossed three times to wild type before further analysis and designated *unc-22(sf21)*.

Whole-genome sequencing

Genomic DNA from *unc-22(sf21)* was prepared and provided to the Emory Integrated Genomics Core (EIGC) for Illumina sequencing. The Genomic Services Laboratory at the HudsonAlpha Institute for Biotechnology performed quality control and constructed standard Illumina sequencing libraries following the manufacturer's instructions. Sequencing was performed on an Illumina Hiseq version 3 with 100–base pair paired-end reads. Raw data were returned to the EIGC for bioinformatics analysis. Raw reads were mapped against the *C. elegans* reference genome (WS190/ce6) with the PEMapper software package. PEMapper maps short reads to a reference genome by first decomposing those reads in *k*-mers (16-mers in this case) and then performing a hash-based "rough mapping" of each read. After roughly mapping the read, the fine-scale position of the read is determined by a local Smith–Waterman alignment. Genotypes were determined using PECaller. Intuitively, we envisioned the six channels of data (number of A, C, G, T, deletion, and insertion reads) as being multinomially sampled, with some probability of drawing a read from each of the channels, but the probability varies from experiment to experiment and is itself drawn from a Dirichlet distribution. PECaller combines data across samples in order to identify the genotype with the highest likelihood at each sequenced base. Both PEMapper and PECaller are part of a custom software package developed at Emory University for mapping and identifying variant sites from Illumina raw sequencing data (D. J. Cutler and M. E. Zwick, personal communication). Analysis then focused on the ~60-kb *unc-22* gene. PECaller

identified a single homozygous mutation specifying the desired KtoA change and no other mutations in the *unc-22* gene.

Immunolocalization

Adult nematodes were fixed as described previously (Nonet *et al.*, 1993; Wilson *et al.,* 2012). Primary antibodies were used at the following dilutions: anti–ATN-1 (α-actinin; MH35; Francis and Waterston, 1991) at 1:200, anti–myosin heavy chain A (MHC A; mouse monoclonal 5-6; Miller *et al.*, 1983) at 1:200, anti-paramyosin (UNC-15; monoclonal 5-23; Miller *et al.,* 1983) at 1:200, anti–PAT-6 (Warner *et al.*, 2013) at 1:200, anti-twitchin (I I II; Benian *et al.*, 1996) at 1:200, and anti–UNC-89 (Benian *et al.,* 1996; rabbit polyclonal EU30) at 1:200. MH35 antibodies were kindly provided by Pamela Hoppe (Western Michigan University). The 5-6 and 5-23 antibodies were obtained from the Developmental Studies Hybridoma Bank (Iowa City, IA). For anti-twitchin and anti-UNC-89, the secondary antibody was anti-rabbit Alexa 488 (Invitrogen). For anti-ATN-1, anti-MHC A, and anti-paramyosin, the secondary antibody was anti-mouse Alexa 594 (Invitrogen). For anti-PAT-6, the secondary antibody was anti-rat Alexa 594 (Invitrogen). Each secondary antibody was used at 1:200 dilution. Images were captured at room temperature with a Zeiss confocal system (LSM510) equipped with an Axiovert 100 M microscope and an Apochromat 63×/1.4 numerical aperture oil objective in 2.5× zoom mode. The color balances of the images were adjusted by using Adobe Photoshop. We examined the staining of at least three worms from each sample.

Electron microscopy

Nematodes were fixed with 2.5% glutaraldehyde in 0.1 M cacodylate buffer (pH 7.4) for 3 h. Samples were then cut in half to allow additional fixation overnight. After washing with 0.1 M cacodylate buffer and postfixing with 1% osmium tetroxide in the same buffer for 1 h, samples were washed with deionized water, dehydrated through an ethanol series, and then placed in 100% ethanol. After two propylene oxide rinses, samples were infiltrated with a mixture of propylene oxide and Eponate 12 resin (Ted Pella, Redding, CA) at a 1:1 ratio overnight and then 1:2 ratio for 6 h. After overnight infiltration in Eponate 12 resin, multiple nematodes were placed in parallel in a small drop of Eponate 12 resin and polymerized in a 60°C oven. On polymerization, the worm halves were reembedded for cross-sectioning. Ultrathin sections were cut 70–80 nm thick with a Leica UltraCut S ultramicrotome (Leica Microsystems, Buffalo Grove, IL). Grids with ultrathin sections were stained with 5% uranyl acetate and 2% lead citrate. The ultrathin sections were imaged on a JEM-1400 transmission electron microscope (JEOL Tokyo, Japan) equipped with a US1000 charge-coupled device camera (Gatan, Pleasanton, CA). Brightness and contrast were adjusted by using Photoshop (Adobe, San Jose, CA).

Swimming assays

For the swimming assays, synchronized young adult animals were transferred into M9 buffer (85 mM NaCl, 42 mM Na_2HPO_4, 22 mM KH_2PO_4 and 1 mM $MgSO_4$). Body bends of individual young adult animals were counted for 1 min. A body bend was scored as a complete deflection of the anterior portion of the nematode from the midline. At least 15 animals of each genotype were analyzed. Values are reported as means and standard errors and tested for significance by Dunnett's test.

Crawling on a plate and optogenetic assays

Crawling on an agar surface (induced backward locomotion) was performed using the methods as described (Hwang *et al.,* 2016; Barnes *et al.,* 2016). Young adult animals were transferred onto a fresh 5.5-cm nematode growth medium (NGM) plate (without bacterial seeding). After a 2-min acclimation period, the front of the animal was gently prodded with a platinum wire to induce backward locomotion, and a movie was recorded. The movie was postprocessed to extract the worm skeleton using custom software written in MATLAB. The velocity of backward crawling was measured and normalized by the length of each worm. For optogenetics assays of muscle kinetics, animals carrying transgene *zxIs6* were grown on NGM plates with OP50 *E. coli* mixed with all-*trans*-retinal for 3.5 d before experiments. Synchronized young adult animals were loaded into multiple parallel microchannels made of an optically transparent elastic polymer, polydimethylsiloxane (PDMS), and trapped by pneumatically controllable PDMS membrane valves (Stirman *et al.,* 2010; Hwang *et al.,* 2016). To induce ChR2 photoactivation, the trapped animals were simultaneously illuminated with blue light (450–590 nm; 0.3 mW/mm^2) for 15 s on the device. For quantitative measurements of a temporal change in projected body area, movies were recorded and postprocessed using custom software written in MATLAB. All curve fitting and statistical analysis were performed using Prism 5 (GraphPad Software). A Wilcoxon rank sum test was conducted for comparison of the data when appropriate.

Competitive fitness assays

Experimental *C. elegans* strains were competed against a GFP-labeled tester strain with an N2 background (JK2735) that was obtained from the *Caenorhabditis* Genetics Center. Ten replicate competition assays were run for the experimental strains, wild-type N2, and *unc-22(sf21)* 3X oc. Competition assays were run for four passages on a 100-mm Petri dish containing 30 ml of NGM-lite (US Biological), seeded with 200 µl of *E. coli* (OP50), and stored at 20°C during competition. Before the assay, nematode lines were bleach-synchronized (Lewis and Fleming, 1995). Competition assays were initially set up at a ratio of 100 experimental L4 larvae to 100 GFP L4 larvae. The larvae were permitted to develop to adults, exhaust the bacterial lawn, and reproduce. Every 4 d (approximately one nematode generation), the entire dish, containing parents and offspring, was washed with 1 ml of M9 buffer, and the nematodes were pelleted. Approximately 1000 nematodes were transferred to a new dish containing OP50, using methods described in Morran *et al.* (2009). After the fourth passage, the frequency of the experimental strain relative to the GFP strain was measured in 200 individuals from a cross-section of the Petri dish to determine the relative fitness of the experimental strain to the GFP strain (Morran *et al.*, 2009). An increase in the frequency of the experimental strain relative to the GFP indicates greater competitive fitness for the experimental strain. In addition, 10 replicates of only JK2735 individuals (no experimental strains) were run to test for the loss of GFP as a control. We observed no loss of GFP expression across all 10 replicates over four passages. Values are reported as means and standard errors. A Kruskal–Wallis nonparametric test was performed in JMP 12 (SAS Institute) on the proportion of experimental strain values measured after four generations to compare the competitive fitness of the experimental strains (N2 vs. *unc-22(sf21)*).

Nicotine sensitivity assays using a WMicrotracker device

The method of nicotine assay was described previously (Matsunaga *et al.*, 2015). Synchronized young adult animals of each genotype were collected in M9 buffer. After a final wash with M9 buffer containing 0.01% Triton X-100 (M9T), a worm slurry (worm pellet: M9T = 1: 5) was prepared. For the assays, 96-well plates were used. To each well was added 40 µl of M9T followed by 10 µl of slurry,

delivering ~50–100 worms/well. The plate was placed in the dark at room temperature for 1 h. Then locomotive activities under no-nicotine conditions were measured for 1 h using a WMicrotracker (Phylumtech) with the program "*C. elegans* (>L4)" supplied by the manufacturer. After the measurement, 50 µl of M9T containing 0.2 or 0.1% nicotine solution was added to each well, and locomotive activities were measured using the WMicrotracker. For each strain and nicotine concentration, eight independent wells were assayed. On the graphs of locomotive activity versus time, each point represents the mean and standard error.

Western blotting

Equal amounts of total protein from wild-type N2 and *unc-22(sf21)* nematodes were separated by 5% polyacrylamide–SDS gels (50 V for 40 min, 100 V for 10 min, and 200 V for 60 min), transferred to nitrocellulose membrane (Bio-Rad Laboratories) using transfer buffer (25 mM Tris-base, 192 mM glycine. and 20% methanol [vol/vol]) at 100 V for 2 h, blocked overnight in 5% skim milk (wt/vol)–TBST buffer (0.1% Tween-20 [vol/vol], 1× TBS, pH 7.6), and reacted with anti-twitchin (Benian *et al.*, 1996) at 1:4000 in the same buffer for 1 h at room temperature. After washing, the blot was incubated with anti-rabbit horseradish peroxidase–conjugated secondary antibody (NA9340; GE Healthcare). The signal from the membrane was obtained using a Pierce ECL Western Blotting Substrate (Thermo Scientific) and HyBlot CL film (Denville Scientific).

Brood-size measurements

Synchronized L4-stage animals were transferred onto 3-cm NGM plates (one worm/plate) with fresh OP50 bacteria. Adult worms were transferred every day (24 h) onto new plates for 6 d. The number of viable progeny from each of these adults was totaled. For each strain, the number of progeny from 15 animals was determined. Values are reported as means and standard errors and tested for significance by Dunnett's test.

Transgenic animals for determining tissue expression of *unc-22* promoters

Four plasmids were created, representing each of the four possible *unc-22* promoters: *unc-22p (ABFGHI)::gfp*, *unc-22p (D)::gfp*, *unc-22p (C)::gfp, and unc-22p (E)::gfp.* PCR was used to amplify, from genomic DNA, 3.0 kb including the putative promoter sequence upstream of *unc-22*, a putative 5′-untranslated region, initiator ATG, and the first 24 nucleotides of coding sequence of *unc-22.* These fragments were then cloned into the pPD_venus vector, which contains a multiple cloning site followed by *venus* coding sequence and *unc-54* 3′-untranslated region, using *Pst*I and *Sma*I sites or *Pst*I and *Msc*I sites. The plasmids were injected at 20 ng/ml into the gonads of wild-type animals along with the pRF4 [*rol-6*(*su1006*)] plasmid as coinjection marker (80 ng/ml; Mello and Fire, 1995). At least three independent stable transgenic lines were generated for each plasmid. Fluorescence and differential interference contrast images were obtained with an Axioskop microscope and AxioCam MR camera (Carl Zeiss).

ACKNOWLEDGMENTS

We thank Dina Greene and Rachel Stanford for their help in making some of the plasmids. G.M.B., H.L., and O.M. gratefully acknowledge support from a Human Frontier Science Program Grant (RGP0044/2012). E.M. was supported in part by the Robert P. Apkarian Integrated Electron Microscopy Core, which is subsidized by the Emory College of Arts and Sciences and the Emory University School of Medicine. Additional support was provided by the National Center for Advancing Translational Sciences of the National Institutes of Health (UL1TR000454). EM images were captured with a JEOL JEM-1400 120kV TEM, which is supported by National Institutes of Health Grant S10 RR025679.

REFERENCES

Ayme-Southgate A, Southgate R, Saide J, Benian GM, Pardue ML (1995). Both synchronous and asynchronous muscle isoforms of projectin (the Drosophila bent locus product) contain functional kinase domains. J Cell Biol 128, 393–403.

Barnes DE, Hwang H, Ono K, Lu H, Ono S (2016). Molecular evolution of troponin I and a role of its N-terminal extension in nematode locomotion. Cytoskeleton 73, 117–130.

Benian GM, Tinley TL, Tang X, Borodovsky M (1996). The Caenorhabditis elegans gene unc-89, required for muscle M-line assembly, encodes a giant modular protein composed of Ig and signal transduction domains. J Cell Biol 132, 835–848.

Bogomolovas J, Gasch A, Simkovic F, Rigden DJ, Labeit S, Mayans O (2014). Titin kinase is an inactive pseudokinase scaffold that supports MuRF1 recruitment to the sarcomeric M-line. Open Biol 4, 140041.

Bogomolovas J, Fleming JR, Anderson BR, Williams R, Lange S, Simon B, Khan MM, Rudolf R, Franke B, Bullard B, *et al.* (2016). Exploration of pathomechanisms triggered by a single-nucleotide polymorphism in titin's I-band: the cardiomyopathy-linked mutation T2580I. Open Biol 6, 160114.

Brenner S (1974). The genetics of Caenorhabditis elegans. Genetics 77, 71–94.

Endicott JA, Noble MEM, Johnson LN (2012). The structural basis for control of eukaryotic protein kinases. Annu Rev Biochem 81, 587–613.

Epstein HF, Thomson JN (1974). Temperature-sensitive mutation affecting myofilament assembly in Caenorhabditis elegans. Nature 250, 579–580.

Francis R, Waterston RH (1991). Muscle cell attachment in Caenorhabditis elegans. J Cell Biol 114, 465–479.

Gieseler K, Qadota H, Benian GM (2016). Development, structure and maintenance of C. elegans body wall muscle. WormBook 13, 1–59.

Greene DN, Garcia T, Sutton RB, Gernert KM, Benian GM, Oberhauser AF (2008). Single-molecule force spectroscopy reveals a stepwise unfolding of Caenorhabditis elegans giant protein kinase domains. Biophys J 95, 1360–1370.

Heierhorst J, Probst WC, Kohanski RA, Buku A, Weiss KR (1995). Phosphorylation of myosin regulatory light chains by the molluscan twitchin kinase. Eur J Biochem 233, 426–431.

Heierhorst J, Tang X, Lei J, Probst WC, Weiss KR, Kemp BE, Benian GM (1996). Substrate specificity and inhibitor sensitivity of Ca2+/S100-dependent twitchin kinases. Eur J Biochem 242, 454–459.

Hwang H, Barnes DE, Matsunaga Y, Benian GM, Ono S, Lu H (2016). Muscle contraction phenotypic analysis enabled by optogenetics reveals functional relationships of sarcomere components in *Caenorhabditis elegans.* Sci Rep 6, 19900 .

Hu LY, Kontrogianni-Konstantopoulos A (2013). The kinase domains of obscurin interact with intercellular adhesion proteins. FASEB J 27, 2001–2012.

Iyer GH, Garrod S, Woods VL, Taylor SS (2005a). Catalytic independent functions of a protein kinase as revealed by a kinase-dead mutant: study of the Lys72His mutant of cAMP-dependent kinase. J Mol Biol 351, 1110–1122.

Iyer GH, Moore MJ, Taylor SS (2005b). Consequences of lysine 72 mutation on the phosphorylation and activation state of cAMP-dependent kinase. J Biol Chem 280, 8800–8807.

Katzemich A, West RJ, Fukuzawa A, Sweeney ST, Gautel M, Sparrow J, Bullard B (2015). Binding partners of the kinase domains in Drosophila obscurin and their effect on the structure of the flight muscle. J Cell Sci 128, 3386–3397.

Konarev PV, Volkov VV, Sokolova AV, Koch MHJ, Svergun DI (2003). PRIMUS: a Windows PC-based system for small-angle scattering data analysis. J Appl Crystallogr 36, 1277–1282.

Kontrogianni-Konstantopoulos A, Ackermann MA, Bowman AL, Yap SV, Bloch RJ (2009). Muscle giants: molecular scaffolds in sarcomerogenesis. Physiol Rev 89, 1217–1267.

Krüger M, Kötter S (2016). Titin, a central mediator for hypertrophic signaling, exercise-induced mechanosignaling and skeletal muscle remodeling. Front Physiol 7, 76.

Krüger M, Linke WA (2011). The giant protein titin: a regulatory node that integrates myocyte signaling pathways. J Biol Chem 286, 9905–9912.
Lange S, Xiang F, Yakovenko A, Vihola A, Hackman P, Rostkova E, Kristensen J, Brandmeier B, Franzen G, Hedberg B, *et al*. (2005). The kinase domain of titin controls muscle gene expression and protein turnover. Science 308, 1599–1603.
Lei J, Tang X, Chambers TC, Pohl J, Benian GM (1994). Protein kinase domain of twitchin has protein kinase activity and an autoinhibitory region. J Biol Chem 269, 21078–21085.
Lewis JA, Fleming JT (1995). Basic culture methods. Methods Cell Biol 48, 3–29.
Liewald JF, Brauner M, Stephens GJ, Bouhours M, Schultheis C, Zhen M, Gottschalk A (2008). Optogenetic analysis of synaptic function. Nat Methods 5, 895–902.
Matsunaga Y, Qadota H, Furukawa M, Choe H, Benian GM (2015). Twitchin kinase interacts with MAPKAP kinase 2 in *Caenorhabditis elegans* striated muscle. Mol Biol Cell 26, 2096–2111.
Mayans O, Benian GM, Simkovic F, Rigden DJ (2013). Mechanistic and functional diversity in the mechanosensory kinases of the titin-like family. Biochem Soc Trans 41, 1066–1071.
Mello C, Fire A (1995). DNA transformation. Methods Cell Biol 48, 451–482.
Miller DM 3rd, Ortiz I, Berliner GC, Epstein HF (1983). Differential localization of two myosins within nematode thick filaments. Cell 34, 477–490.
Moerman DG, Baillie DL (1979). Genetic organization in *C. elegans*: fine-structure analysis of the *unc-22* gene. Genetics 91, 95–103.
Moerman DG, Benian GM, Barstead RJ, Schriefer LA, Waterston RH (1988). Identification and intracellular localization of the *unc-22* gene product of *Caenorhabditis elegans*. Genes Dev 2, 93–105.
Morran LT, Parmenter MD, Phillips PC (2009). Mutation load and rapid adaptation favour outcrossing over self-fertilization. Nature 462, 350–352.
Nonet ML, Grundahl K, Meyer BJ, Rand JB (1993). Synaptic function is impaired but not eliminated in *C. elegans* mutants lacking synaptotagmin. Cell 73, 1291–1305.
Paix A, Folkmann A, Rasoloson D, Seydoux G (2015). High efficiency, homology-directed genome editing in *Caenorhabditis elegans* using CRISPR-Cas9 ribonucleoprotein complexes. Genetics 201, 47–54.
Petoukhov MV, Franke D, Shkumatov AV, Tria G, Kikhney AG, Gajda M, Gorba C, Mertens HDT, Konarev PV, Svergun DI (2012). New developments in the ATSAS program package for small-angle scattering data analysis. J Appl Cryst 45, 342–350.
Petoukhov MV, Konarev PV, Kikhney AG, Svergun DI (2007). ATSAS 2.1 – towards automated and web-supported small-angle scattering data analysis. J Appl Cryst 40, s223–s228.
Qadota H, McGaha LA, Mercer KB, Stark TJ, Ferrara TM, Benian GM (2008). A novel protein phosphatase is a binding partner for the protein kinase domains of UNC-89 (Obscurin) in *Caenorhabditis elegans*. Mol Biol Cell 19, 2424–2432.
Rambo RP, Tainer JA (2013). Accurate assessment of mass, models and resolution by small-angle scattering. Nature 496, 477–481.
Stirman JN, Brauner M, Gottschalk A, Lu H (2010). High-throughput study of synaptic transmission at the neuromuscular junction enabled by optogenetics and microfluidics. J Neurosci Methods 191, 90–93.
von Castelmur E, Strumpfer J, Franke B, Bogomolovas J, Barbieri S, Qadota H, Konarev PV, Svergun DI, Labeit S, Benian GM, *et al*. (2012). Identification of an N-terminal inhibitory extension as the primary mechanosensory regulator of twitchin kinase. Proc Natl Acad Sci USA 109, 13608–13613.
Warner A, Xiong G, Qadota H, Rogalski T, Vogl AW, Moerman DG, Benian GM (2013). CPNA-1, a copine domain protein, is located at integrin adhesion sites and is required for myofilament stability in *Caenorhabditis elegans*. Mol Biol Cell 24, 601–616.
Wilson KJ, Qadota H, Benian GM (2012). Immunofluorescent localization of proteins in Caenorhabditis elegans muscle. Methods Mol Biol 798, 171–181.
Yochem J, Gu T, Han M (1998). A new marker for mosaic analysis in *Caenorhabditis elegans* indicates a fusion between hyp6 and hyp7, two major components of the hypodermis. Genetics 149, 1323–1334.